



Structural Characteristics, Optical, Transport and Magnetic Properties of Zinc Doped Cobalt Chromium Ferrite Prepared by Co-precipitation Method



A. M. Moustafa*, A. F. Hegab, S. A. Gad and S. M. Shalaby

Solid State Physics Department, Physics Division, National Research Centre, Dokki, Cairo, Egypt, 12622.

A SERIES of zinc doped cobalt chromium ferrite $\text{Co}_{1-x}\text{Zn}_x\text{Fe}_{1.5}\text{Cr}_{0.5}\text{O}_4$ (where $0 \leq x \leq 1$) were synthesized by co-precipitation technique. Structural, optical, transport and magnetic properties were characterized by X-ray diffraction (XRD), di-use reflectance, AC electrical properties and hysteresis loop. XRD analysis indicates that all samples consist of a single-phase cubic spinel structure. Rietveld refinement results indicated an increase in lattice parameter due to the replacement of Co^{2+} by Zn^{2+} and migration of Fe^{3+} ions from A-site to B-site. Optical energy band gaps were calculated and it was found that both E_{g1} and E_{g2} increase with increasing Zn content. Dielectric constant ϵ , ϵ' , and dielectric loss tangent $\tan\delta$ were measured at room temperature as a function of applied frequency and temperature. It was noticed, that ϵ and ϵ' increase with temperature increment and decrease with increasing frequency and this anomaly can be explained by Maxwell Wagner two-layer model. Magnetic measurements revealed that the saturation magnetization increases as Zn content increases up to $\text{Zn}=0.4$ and after that, the saturation magnetization decreases.

Keywords: Spinel Ferrite, Structural Characteristics, Optical Properties, Transport properties, Magnetic Properties.

Introduction

Spinel ferrites exhibit interesting structural, electrical and magnetic properties which leads it to be used in different areas [1,2] such as permanent magnets magnetic fluids, magnetic refrigeration, electromagnetic data storage, sensor, magnetic recording media, switches, microwave devices, isolator circulator, phase shifter computer peripherals, power transformer, telephone and telecommunication system [3,4]. Spinel ferrites, CoFe_2O_4 is an interesting and most attractive material because of its high coercivity, moderate saturation magnetization and most chemical stability that makes it available for the use of recording media [5].

Soft ferrite like substituted cobalt ferrite characterized by low magnetic coercivity and high sensitivity make it magnificent materials for power

transformer in electronic and telecommunication applications [6,7]. Ferrite materials can be prepared in the form of ultrafine particles by different methods like Sol-gel, hydrothermal and Co-precipitation [8, 9]. However, control of particle size in nanometric range by the variation of synthesis condition is always a difficult task. The task of many works was to prepare nanocrystalline Co-ferrite materials by different methods and by making various substitution like Zn, Mn, Ni, Al, Cr, etc., to find an optimum ferrite belongs to spinel structure which exhibits complex disordered phenomena involving the two cation sites. In this respect, spinel group is fundamental to any theory of cation distribution. The determination of the cation distribution between the tetrahedral and octahedral sublattices in spinels is the more interesting and continuous problems in crystal chemistry [10]. To a good approximation, the chemical bonding in spinel

*Corresponding author e-mail: aishamoustafa@yahoo.com

Received ;27/04/2020; Accepted: 07/06/2020

DOI: 10.21608/EJCHEM.2020.28861.2619

©2020 National Information and Documentation Center (NIDOC)

ferrites may be taken as purely ionic. Energy calculations show that the size and valance of cations and parameter of oxygen anions are important factors to govern the cation distribution in spinel structure. Large divalent ions tend to occupy tetrahedral sites as polarization effects favor it. If tetrahedral site ions have lower valency, the intermediate O^{2-} ion becomes polarized towards octahedral site. Thus, polarization favors normal spinel configuration. However, these factors alone cannot give a consistent picture of the observed cation distribution in ferrites and in general in spinel structures. For an instant, $CoFe_2O_4$ is an inverse spinel, while $ZnFe_2O_4$ crystallizes in normal spinel, although Zn^{2+} and Co^{2+} have nearly the same ionic radii. Therefore, the need is to determine the cation distribution, by utilizing the structure refinement using x-ray technique.

The preparation conditions, the structure as well as transport and magnetic properties facilitate cobalt ferrite usage in many applications like magnetic recording, data storage and other Nano electronics. By studying AC, electrical properties under the effect of temperature and composition can provide us with precious information of restricted electric charge carriers and this will lead to good understanding the mechanism of electric conduction. This study aims to providing the correlation between the structural characteristics (unit cell dimension, cation distribution, bond lengths, and crystallite size) and both of the optical, transport and magnetic properties.

Experimental Procedure

A series of Zn substituted cobalt ferrite $Co_{1-x}Zn_xFe_{1.5}Cr_{0.5}O_4$ (where $0.0 \leq x \leq 1.0$) prepared using co-precipitation method [9]. Nitrates of the constituent cations of highly pure materials were used for preparation of the corresponding hydroxides according to the scheme 1:

The dried precipitation was pressed into discs under pressure of 15 Tons/cm² and calcined in air at 800°C for 6 hours. The fired sample was tested by X-Ray diffraction, indicating, and the formation of the desired ferrite sample together with oxides of the constituents. Presintered discs were grounded into fine powder and pressed again into discs under same pressure and followed by sintering in air at 1300 °C, for 48 hours with a rate of heating 4°C/Min. X-ray diffraction data were collected on Diano diffractometer using step scanning mode and filtered $Co\ k_{\alpha}$ radiation. The scanning range was between 15° and 100° “2θ”

with a step size of 0.05° and count time of 10 sec/step. Diffuse reflection measurements were done in the wavelength range from 600 to 1200 nm using Jasco (V-570) spectrophotometer.

The electrical measurements were done on RLC Bridge (Hioki model 3531 made in Japan) from ambient temperature up to 700K at different frequencies (100 Hz - 5000 kHz). ϵ was calculated by using the formula:

$$\epsilon = \frac{cd}{_0A} \quad (2)$$

Where ϵ , ϵ_0 , c, d and A are the real part of dielectric constant, constant of permittivity of free space, capacitance of pellet, thickness and cross-sectional area of flat surface. A vibrating sample magnetometer model 9600-1-VSM was used for the magnetic properties measurements.

Results and Discussion

Structural Analysis

X-Ray diffraction patterns of synthesized $Co_{1-x}Zn_xFe_{1.5}Cr_{0.5}O_4$, ($0.0 \leq x \leq 1.0$) compounds are shown in Fig. (1a). From this figure, it is clearly showed that all samples formed in single phase cubic structure matched with ICDD card no. 88-2152 with no additional lines corresponding to any other phases of elements oxides or binary oxides along the whole, measured 2 θ ranges. Prepared samples were successfully refined using Rietveld method implemented in fullprof program [11].

The starting model was spinel structure of space group Fd3m (no. 227) with origin at center ($\bar{3}m$) and Wycoff notation for A- site (8a) of point symmetry ($\bar{4}3m$), B- site (16d) of point symmetry ($\bar{3}m$) and O- site (32e) of point symmetry (3m). The cation distributions of samples under study were first performed based on preference site of each cation. As reported in the literature [12,13], Cr and Co cations prefer to occupy B- site while Zn cation prefers A- site. Accordingly, the first sample of $Co_{1-x}Zn_xFe_{1.5}Cr_{0.5}O_4$ series, where $x=0$, the cations have been distributed as follows: Cr and Co occupy B-site and Fe has been distributed among B-site and A-site to form inverted spinel as input model to carry out the structure refinement. It is worth mentioning, that the five other samples with $x > 0$, Zn cation was put in its preference A-site.

The global parameters were refined at first followed by the structure parameters in sequence mode. When the discrepancy factors has reached its minimum value all parameters (global and

structural) were refined simultaneously giving goodness of fit index, $c^2 = (R_{wp}/R_{exp})^2$ as shown in Table 1. It is clearly shown from R_w and c^2 values that the refined structural parameters are reliable. Agreement between observed and calculated diffraction profiles of sample 2 as an example is shown in Fig. 1b.

All results obtained from the refinement are tabulated in Table (1). A relation between refined values of lattice parameter "a" and zinc content "x" is shown in Fig.2, it exhibit a linear content dependence, thus obeying Vegard's law [14, 15] which implies the formation of homogeneous $Co_{1-x}Zn_xFe_{1.5}Cr_{0.5}O_4$ solid solution. Such a remarkable

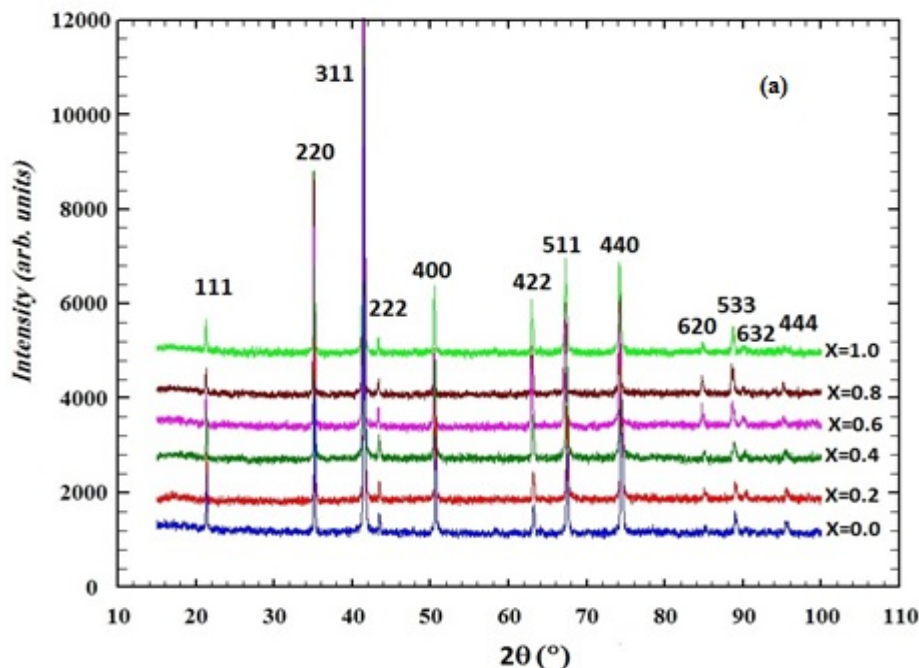


Fig. (1a).): X-ray Powder diffraction patterns of $Co_{1-x}Zn_xFe_{1.5}Cr_{0.5}O_4$, $0.0 \leq x \leq 1.0$.

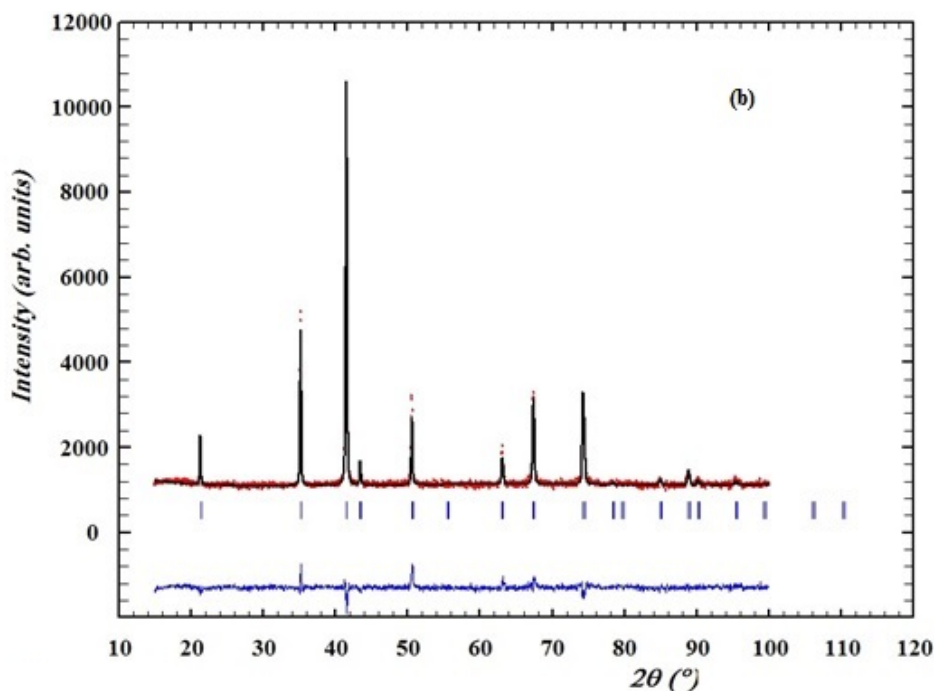
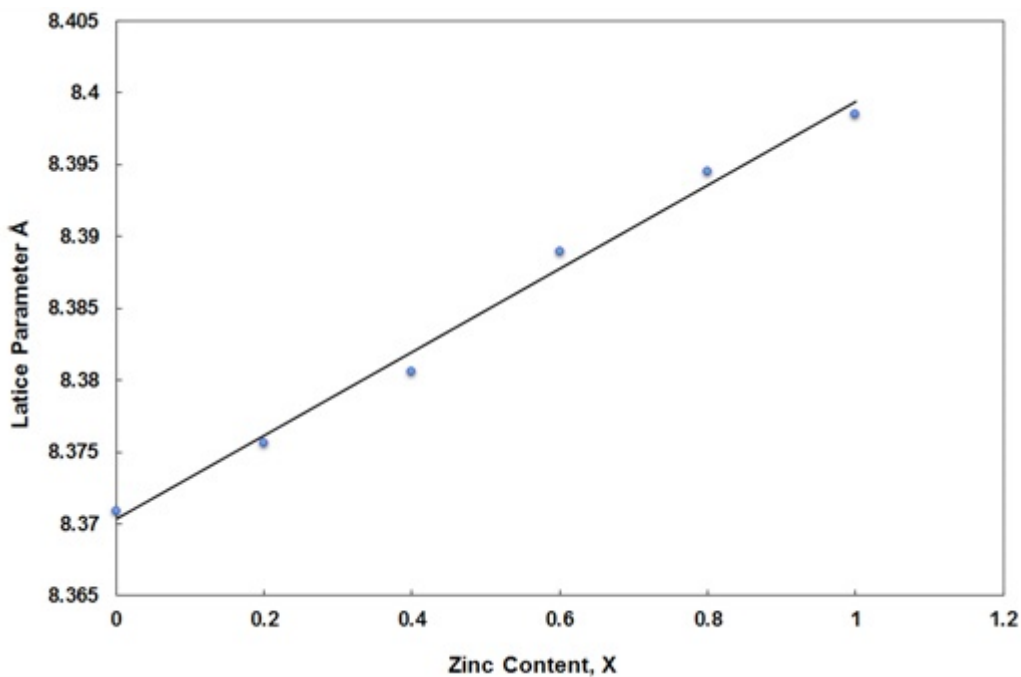


Fig.(1b). Rietveld refined XRD pattern of powder samples $Co_{0.8}Zn_{0.2}Fe_{1.5}Cr_{0.5}O_4$.

TABLE 1. The atomic positions coordinates (x, y, z), occupancy (g), the discrepancy factors, crystallite size and microstrain.

Atoms	Zn=0.0		Zn = 0.2		Zn = 0.4		Zn = 0.6		Zn = 0.8		Zn = 1.0	
	x=y=z	g	x=y=z	g	x=y=z	g	x=y=z	g	x=y=z	g	x=y=z	g
O	0.2545	4.0	0.2561	4.0	0.2617	4.0	0.2554	4.0	0.2569	4.0	0.2592	4.0
Cr	0.5000	0.5	0.5000	0.5	0.5000	0.5	0.5000	0.5	0.5000	0.5	0.5000	0.5
Fe	0.5000	1.343	0.5000	1.5	0.5000	1.5	0.5000	1.5	0.5000	1.5	0.5000	1.5
Co	0.5000	0.157	0.5000	0.0	0.5000	0.00	0.5000	0.00	0.5000	0.00	0.5000	0.00
Fe	0.1250	0.157	0.1250	0.0	0.1250	0.00	0.1250	0.00	0.1250	0.00	0.1250	0.00
Co	0.1250	0.843	0.1250	0.8	0.1250	0.6	0.1250	0.4	0.1250	0.2	0.1250	0.00
Zn	0.1250	0.00	0.1250	0.2	0.1250	0.4	0.1250	0.6	0.1250	0.8	0.1250	1.0
R_{wp}	18.9		19.3		19.8		24.0		22.7		23.5	
R_{exp}	14.8		15.1		14.7		14.4		14.7		16.1	
χ^2	1.625		1.637		1.816		2.801		2.388		2.132	
Microstrain %	0.3192		0.3596		0.4611		0.5069		0.5576		0.2934	
Crystallite size nm	139		146		163		238		194		116	

χ^2 is the goodness of fit index $\chi^2 = (R_{wp}/R_{expected})^2$.

Fig. 2. Rietveld refined XRD pattern of powder samples $Co_{0.8}Zn_{0.2}Fe_{1.5}Cr_{0.5}O_4$.

change in lattice parameter may be attributed to the fact that Goldsmith ionic radius of Zn^{2+} (0.60 Å) is higher than that of Co^{2+} (0.58 Å). Consequently, replacement of Co^{2+} by Zn^{2+} point out an increase in lattice parameter. A.V. Raut *et al.* [16] have obtained same behavior. Now, it is worth mentioning, that the small difference between ionic radii of Co^{2+} and Zn^{2+} is not matching the increase in the unit cell parameter for these compounds. Hence, there is another reason, in addition to the difference in ionic radii, responsible for this increment. A. M. Moustafa *et al.* found that [17], when cation of higher valence replaces lower valence one, there will be a vacant site as is required to keep charge neutral. Now, taking into consideration the cations occupancy values obtained tabulated in Table 1. So the second reason responsible for the increase in lattice parameter, for sample with $x=0.0$, which is partially inverted spinel structure (Fe^{3+} distributed between B & A sites) therefore the divalent Co^{2+} distributed between B & A sites, as shown in Table (1), leads to the predication of vacant sites, and consequently the smallest lattice parameter has attained. From sample “2”, where $x=0.2$, up to $x=1.0$, which are normal spinel, the vacant sites reduced to a minimum value which leads to an increase in lattice parameter. It is clearly noticed that the introduction of Zn^{2+} ions into the structure chemically, at the expense of Co^{2+} ions, will help in migration of Fe^{3+} ions in A- site to B- site and catalyzes the formation of normal spinel structure.

It has been reported in literature, that $CoFe_2O_4$ is not completely inverse, and the degree of inversion depends on heat treatment [18]. Ratio of Fe (A)/ Fe (B) has been found to vary from 0.61 to 0.87 in $CoFe_2O_4$ by two extreme heat treatments, quenching and slowly cooling respectively. But, the result of our investigated sample $CoFe_{1.5}Cr_{0.5}O_4$, the divalent cation is only Co^{2+} , the ratio of Fe(A)/Fe(B), according to results of occupancy, Table 1, is equal to 0.118 much less relative to the prementioned ratio. This finding may be attributed to presence of Cr^{3+} ion in B-site, which helps in migration of Fe^{3+} ions from A-site to B-site and the same number of Co^{2+} ions moved from B-site to A-site. On the other hand, for Co- ferrite substituted with Zn^{2+} ion, it has been reported [19] that the cation distribution of $(Co_{0.9}Zn_{0.1}Fe_2O_4)$ is $[Zn_{0.1}Co_yFe_{1-y}]^A [Co_{0.9-y}Fe_{1+y}]^B O_4$, indicating that yFe^{3+} ions have migrated from A to B sites (the same number of Co^{2+} ions moved from B sites to A sites). This expectation has been emphasized by studying Mössbauer spectra of

this compound and reaching to the conclusion, that the increase in Zn^{2+} concentration increases ionic migration of Fe^{3+} ions from A sites to B sites. These findings are completely consistent with our results, where our investigated samples with $x \geq 0.2$ are considered to be completely normal spinel structure as indicated from the values of the occupancy in A and B sites. The only difference is the high emigration of Fe^{3+} ions from A-site to B-site and Co^{2+} ions from B-site to A-site as Zn^{2+} concentration is increased ($x \geq 0.2$) and consequently this leads to normal spinel structure of these compounds. Also, in view of the well-known preference of Cr^{3+} ions to occupy octahedral sites, it may be assumed that it is responsible for migration of Co^{2+} ions to tetrahedral sites besides the effect of Zn^{2+} ions. Therefore, cation distribution of the investigated compounds $Co_{1-x}Zn_xFe_{1.5}Cr_{0.5}O_4$ with $x \geq 0.2$ is $(Co_{1-x}Zn_x)^A (Fe_{1.5}Cr_{0.5})^B O_4$.

Crystallite size values tabulated in Table (1) and depicted in Fig.3a indicated that there is gradual increase followed by decrease at sample number 4 where $x = 0.6$ as Zn increases. Approximately the same behavior is also observed in the Fig. 4b relating the strain by Zn content. This behavior may be attributed to mutual effect of lattice parameters and the surface phenomena [20]. The variation of lattice parameters and crystallite size was explained either in terms of outward relaxation at crystal faces so that some interplaner spacings are appreciably distorted or on the basis of surface tension considerations [21, 22]. The interpretation depends on the sign of the surface energy [23]. On the other hand, the non-uniform strain determined from the broadening of XRD lines as shown in Fig.(3b), while macrostrain caused by the change in an interplaner spacings (d-values) determined from the relative lattice parameter deviation, $\Delta a / a_0$. Figure (4a) shows the behavior of $\Delta a / a_0$ with Zn^{2+} . It is clearly observed that $\Delta a / a_0$, which is the measure of macrostrain, increases linearly with increasing Zn^{2+} content. Same behavior is nearly observed for microstrain (except for sample no.6 where Zn^{2+} cations occupy tetrahedral site only). This linear increase of macrostrain with increment of Zn^{2+} content is expected because the lattice parameter is linearly increased as Zn^{2+} content increases as explained before. However, on the other hand, the relation between lattice parameter and crystallite size behaves differently. That, there is an increase in crystallite size as the lattice parameter increases until sample with ($Zn^{2+} = 0.6$) where a sudden

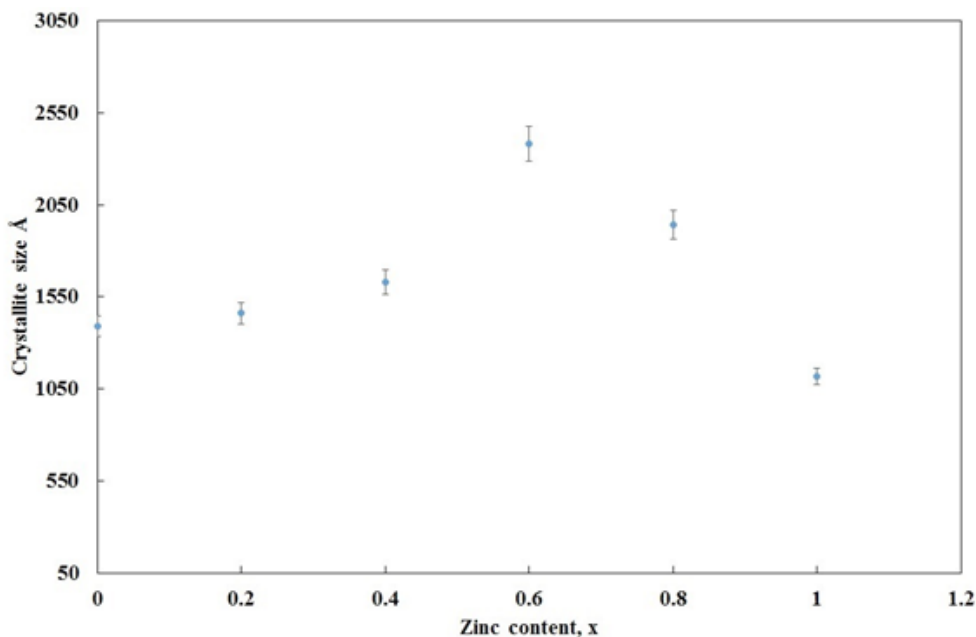


Fig.(3a): Relation between crystallite size and Zn atomic content.

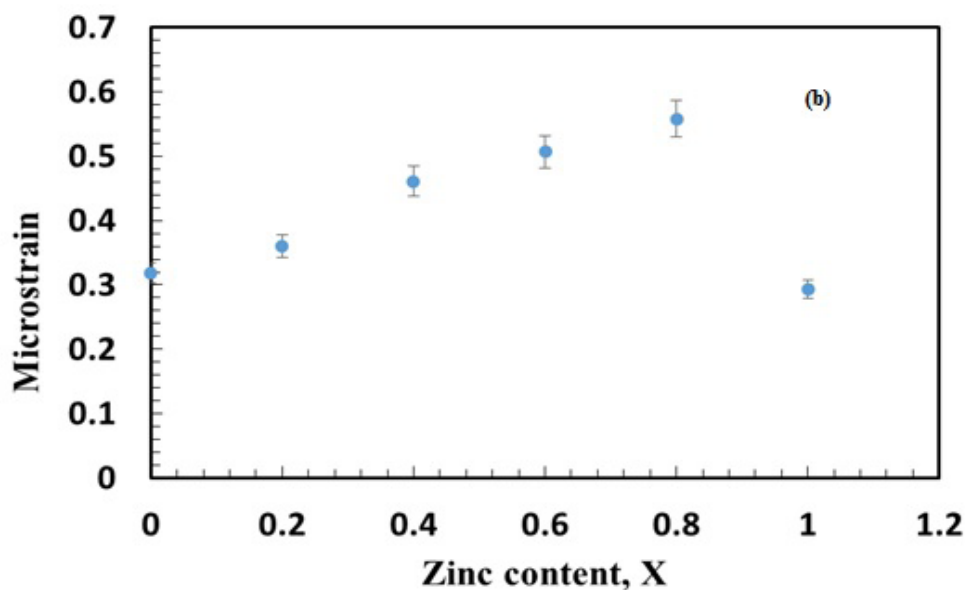


Fig.(3b): Relation between micro strain size and Zn atomic content.

decrease in crystallite size is observed; this is clearly shown in Fig. (4b).

It is better to explain this anomaly by considering the surface energy concept [24], for spherical crystallite of diameter “D” and surface energy “U”, the internal pressure of crystallite size is equal to “4U/D”. This should lead to uniform strain (ϵ), and consequently to the change in lattice parameter given by:

$$3\Delta a/a_0 = -4U/3ED \quad (3)$$

Where “E” is bulk modulus of elasticity.

From this equation, it is noticed, that the decrease or increase in the crystallite size with the lattice parameter depends on the sign of the surface energy “U”. Therefore, the slope of the line relating “1/D” and the lattice parameter indicates

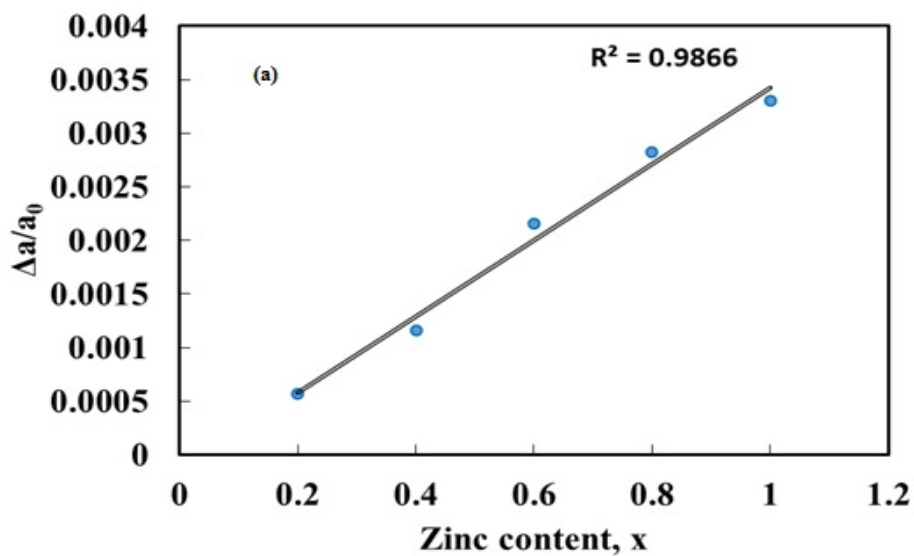


Fig. (4a): Relation between relative lattice parameter size and Zn atomic content.

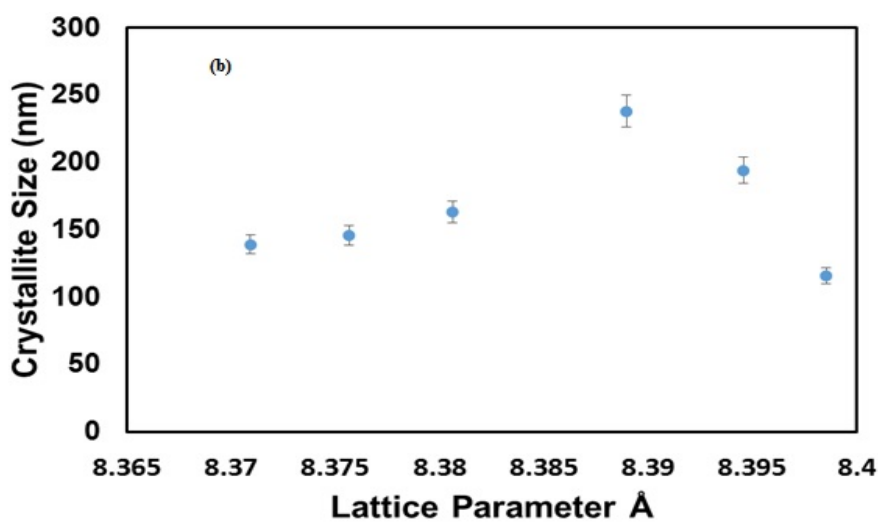


Fig. (4b): Relation between crystallite size and lattice parameter.

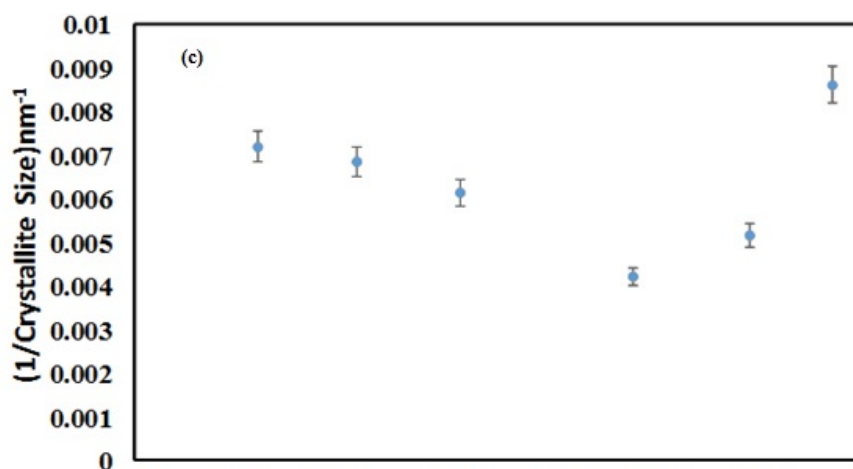


Fig. (4c): Relation between the reciprocal of crystallite size and lattice parameter .

whether surface phenomenon is surface tension (-ve slope) or outward surface relaxation (+ve slope) [18]. Figure (4c) shows a relation between reciprocal of crystallite size as a function of lattice parameter of samples. The figure is characterized by two slopes, negative one for samples from 1 to 4, which the phenomenon may be interpreted in terms of surface tension, and a positive one from samples 4 to 6, which may be interpreted as outward surface relaxation. This may explain the steady state of crystal lattice because there is only one sort of cation, in the tetrahedral sites or because the structure becomes normal spinel.

Table (2) shows calculated lattice distances between cation sites and anion sites using anion parameter and the lattice parameter as given in Table (1). It is clearly shown from the calculated values of lattice distances of tetra- tetra (A-A) of samples are increased by increasing Zn concentration. This behaviour may be attributed to two reasons, the first is the substitution of Co^{2+} of small size (0.58\AA) by Zn^{2+} of larger size (0.60\AA), and the second reason is due to the enlargement of the cell parameter as a function of Zn content. The same reason may describe the same attitude for the octa- octa (B-B) and tetra- octa (A-B) distances because, the interchange of "Co" in the octa-site by the Fe in the tetra site. Moreover, the migration of Fe from the tetra- site to octa- site by increasing the "Zn" content, beside the increment of the lattice parameter will lead to this increment as shown in Table (2).

Taking into consideration the values of the bond lengths A-O and B-O, it has been shown,

that, as shown in Table (2), this result is consistent with the fact, that the preponderance of spinel structures with oxygen parameter u increases from its ideal value ($u > 0.25$), anions move away from the tetrahedrally coordinated A-site along the $\langle 111 \rangle$ directions, which increases the volume of each A- site, while the octahedral B-site become correspondingly small. In general, the tetrahedral sites are isolated from each other with bridge anion with the neighboring octahedral site. No edge sharing between A-site and other A or B sites. However, B-site octahedral shares six of twelve O-O edges. The variations in length of the shared and unshared edges are obvious from the result of calculations Table (2), that the shared edges are shorter than the unshared ones. In addition to the refined atomic position parameter of oxygen u , provides a measure of the level of distortion in the spinel lattice in an undistorted lattice $u=0.25$, while u generally in the range 0.25-0.26 in real ferrites. Refined values of u for six ferrite samples 0.2545 (1) -2617(3).

Optical properties

Optical properties of $\text{CO}_{1-x}\text{Zn}_x\text{Fe}_{1.5}\text{Cr}_{0.5}\text{O}_4$ ($0 \leq x \leq 1$) were analyzed by diffuse Reflectance (DR %) measurements in a wavelength region of 200–2000 nm as shown in Figure 5. Energy band gap (E_g) of all samples was estimated based on optical absorption relation given below [25-27]:

$$F(R_{\infty}) = (B(h\nu - E_g)^n) / h\nu = a \quad (4)$$

Where is Kubelka- Munk equation, is a diffuse reflectance ratio between reference and measured samples, B , $h\nu$ is constant, photon energy, and n defines types of electronic transitions. T_{auc}

TABLE 2. Bond lengths calculated from the obtained refined values.

Bond Length Å	Samples					
	X=0.0	X=0.2	X=0.4	X=0.6	X=0.8	X=1
(A-A)	3.6247	3.6268	3.6289	3.6325	3.6350	3.6367
(A-B)	3.4704	3.4724	3.4744	3.4779	3.4802	3.4819
(B-B)	2.9595	2.9612	2.9630	2.9659	2.9679	2.9693
(A-O)	1.8776	1.9013	1.9850	1.8952	1.9177	1.9527
(B-O)	2.0557	2.0444	2.0015	2.0527	2.0424	2.0250
Tet-edge	2.9605	2.9630	2.9695	2.9673	2.9702	2.9734
Shared octa-edge	2.8530	2.8177	2.6845	2.8371	2.8043	2.7498
Unshared octa-edge	3.0661	3.1048	3.2415	3.0948	3.1315	3.1888

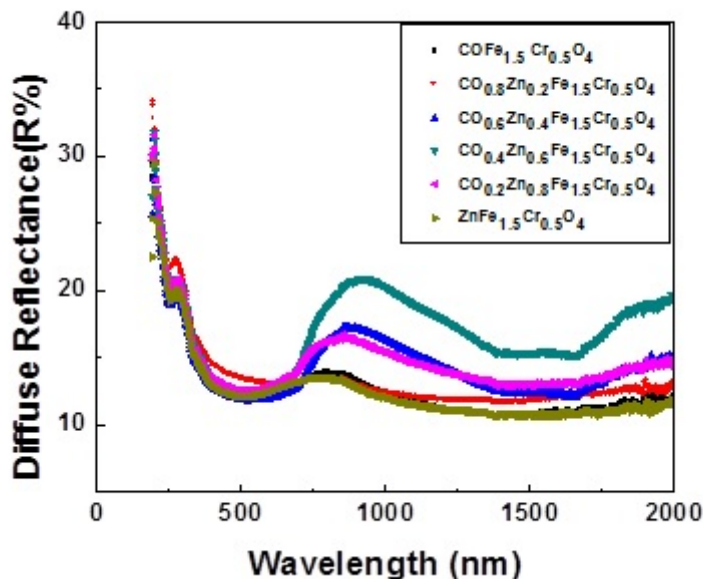


Fig. (5) : Diffuse reflectance vs. wavelength for Co1-x ZnxFe1.5Cr0.5O4 (0 ≤ x ≤ 1).

equation is used to estimate the optical energy band gap (E_g) of the investigated samples [28].

$$ahv=B(hv-E_g)^n \tag{5}$$

Fig.6 (a-f) shows a relation between $(\alpha hv)^2$ and (hv) . Direct energy gap values (E_g) for samples are determined by extrapolating the linear part of $(\alpha hv)^2$ against (hv) plots for $(\alpha hv)^2$ equals to zero eV. From this figure, it is noticed that there are two energy band gaps (E_{g1} , E_{g2}). The dependence of E_{g1} and E_{g2} on Zn content is shown in Fig.7. It is noticed that both E_{g1} and E_{g2} increase with increasing Zn content till $x=0.8$ and then decrease at $x=1$. This increment may be attributed to an energy band gap is influenced by different factors, such as crystallite size, structural parameter, and impurities. In addition, to a certain degree optical band gap could be affected by presence of localized electronic states in the sample. Moreover, due to ionic radius of Zn^{2+} (0.60Å) is higher than that of Co^{2+} (0.58Å). Refractive index (n) evaluation is very important to describe and design optical devices. Also, n of a semiconductor is totally dependent on its band gap. n of ferrite is derived by using Moss and Vandamme's empirical relation [29-31]:

$$E_g n^4=d \tag{6}$$

Where E_g is energy band gap and d is a constant with a value of 108 eV. And Vandamme's empirical relation:

$$n=\sqrt{(1+(A/(E_g+C))^2)} \tag{7}$$

Where $A=13.6$ eV and $C=3.4$ eV. Ravindra et al. [32] have suggested a linear relation prevalent a variation of n with E_g between bonding and antibonding as following:

$$avindra(n)=4.08-0.62E_g \tag{8}$$

Anani et al. [33] have also proposed an empirical relationship between n and E_g of solids as follows:

$$Anani(n)=(17-E_g)/5 \tag{9}$$

Relation between n and E_g is shown in Fig.8 (a, b). We can calculate optical dielectric constant (ϵ_∞) with n by using the following relation:

$$\epsilon_\infty=n^2 \tag{10}$$

ϵ_∞ values which calculated by different methods are tabulated in Table (3).

Transport Properties

Dielectric Properties

Figure (9a) illustrates the relation between real part of dielectric constant (ϵ') and absolute temperature at different frequencies (n) for $CoFe_{1.5}Cr_{0.5}O_4$. From this figure, it is clear that, the general trend can be divided into three regions with respect ton. In first region, ϵ' values are nearly stable with increasing temperature up to 400K. High values of ϵ' at low n region mean that the electronic polarization needs a very small electric field to take place and accordingly increase ϵ' value. In the second region, ϵ' increases and reach

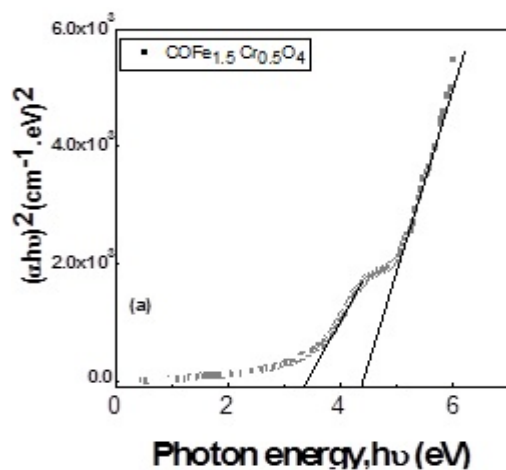


Fig. (6a)

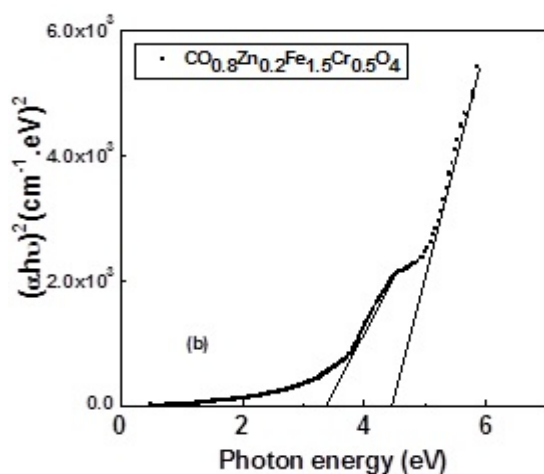


Fig. (6b)

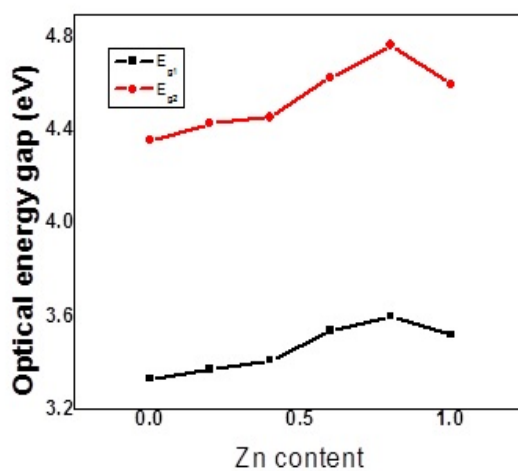
Fig. 6(a - f): Plots of $(\alpha h\nu)^2$ vs. photon energy ($h\nu$) for $\text{Co}_{1-x}\text{Zn}_x\text{Fe}_{1.5}\text{Cr}_{0.5}\text{O}_4$ ($0 \leq x \leq 1$).

Fig.7 : Optical energy band gaps against Zn content.

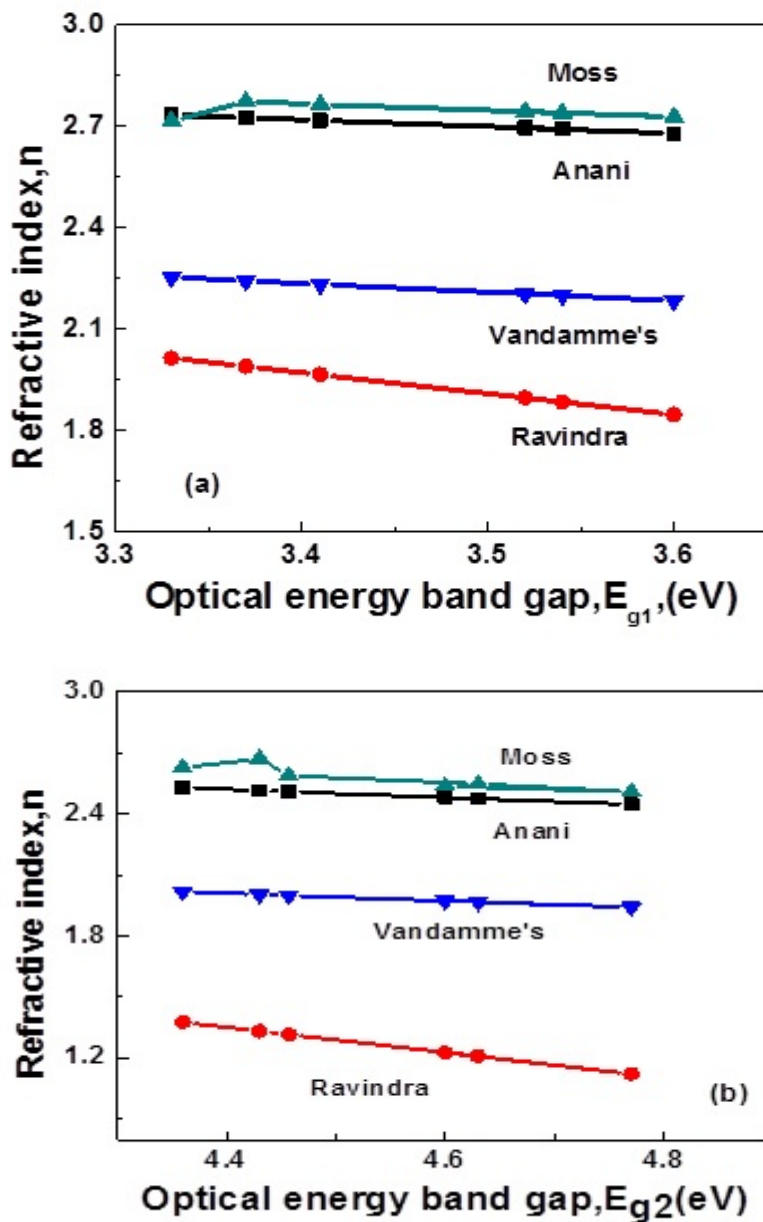


Fig.8 (a,b): Refractive index against optical energy band gap.

TABLE 3. Optical dielectric constants estimated by Anani, Ravindra, Moss and Vandamme's and Vandamme's.

x	$\epsilon_{\infty 1}$ (Anani)	$\epsilon_{\infty 1}$ (Ravindra)	$\epsilon_{\infty 1}$ (Moss and Vandamme's)	$\epsilon_{\infty 1}$ (Vandamme's)	$\epsilon_{\infty 2}$ (Anani)	$\epsilon_{\infty 2}$ (Ravindra)	$\epsilon_{\infty 2}$ (Moss and Vandamme's)	$\epsilon_{\infty 2}$ (Vandamme's)
0	7.474	4.061	7.378	5.083	6.391	1.895	6.899	4.071
0.2	7.431	3.962	7.695	5.035	6.32	1.778	7.132	4.017
0.4	7.387	3.864	7.651	4.988	6.29	1.734	6.688	3.996
0.6	7.246	3.553	7.507	4.841	6.12	1.463	6.489	3.868
0.8	7.182	3.415	7.447	4.774	5.983	1.261	6.289	3.771
1	7.268	3.602	7.529	4.862	6.15	1.508	6.434	3.89

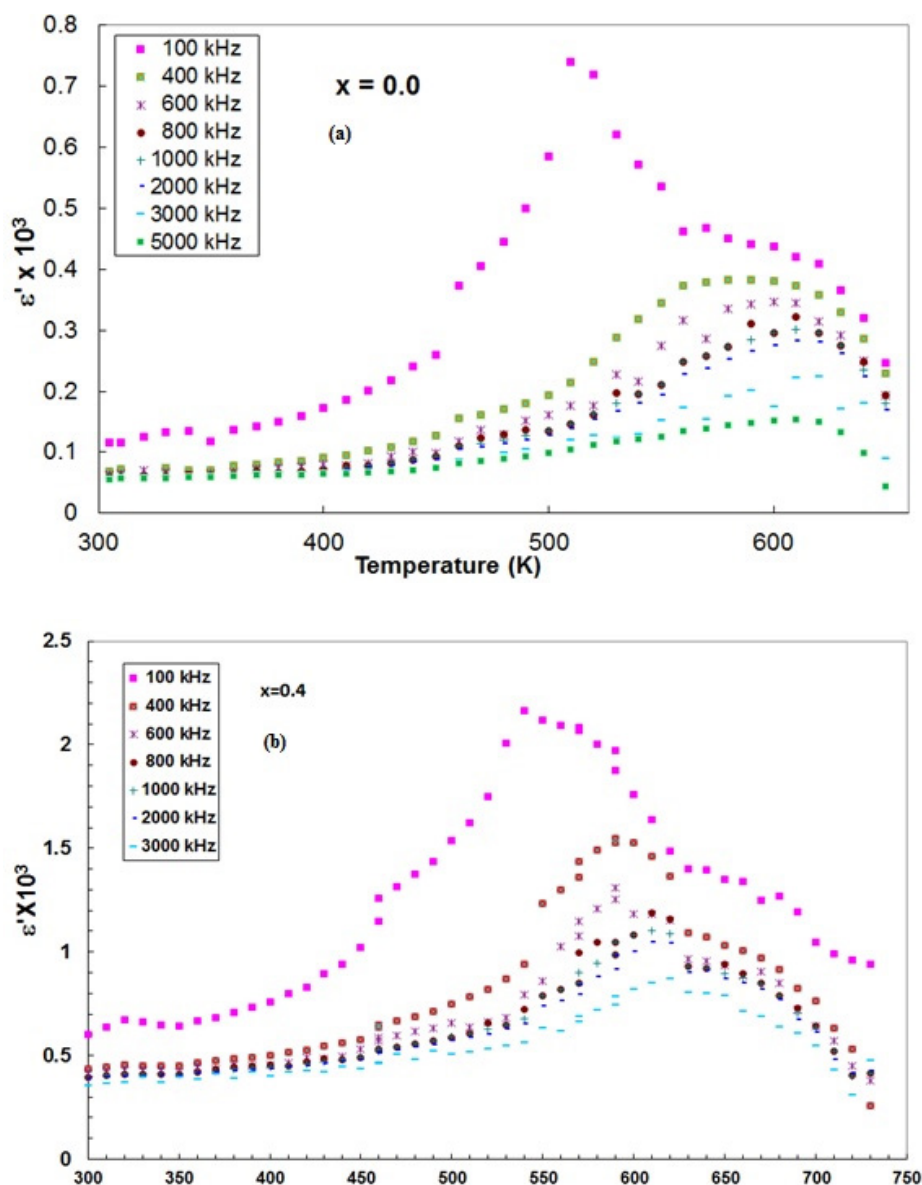


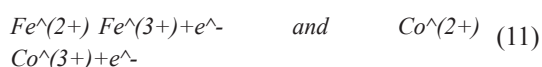
Fig. (9a,b): Relation between Dielectric constant and absolute temperature for the sample $\text{Co}_{1-x}\text{Zn}_x\text{Fe}_{1.5}\text{Cr}_{0.5}\text{O}_4$, with $x=0.0, 0.4$ at different frequencies.

a maximum value at $\approx 450\text{K}$, which may be considered as transition temperature and may be close to Curie temperature. The point of maximum varies depending on applied “ n ”. In third region, ϵ' decreases due to overcoming thermal energy given to the sample during heating to the effect of applied electric field. From a close look, one can find that ϵ' decreases with increasing “ n ”. This is because, at high “ n ”, the dipoles cannot pursuit the field alteration. The variation, as well as a decrease in values of dielectric constant, is the general attitude for dielectric materials and this may be attributed to scattering of charge carriers at high “ n ”. Moreover, the fast variation of electric

field with applied “ n ”, lead to random orientation of electric dipole moments which consequently decreases the value of ϵ' . In other words, this behavior could be explained by electron hopping. In the partial inverse spinel $\text{CoFe}_{1.5}\text{Cr}_{0.5}\text{O}_4$ it is known, that Co^{2+} ions and most of Fe^{3+} ions are randomly distributed over B sites while A sites are occupied by remaining Fe^{3+} , with the oxygen ions in B sites forming a cubic array in the structure. A high concentration of $\text{Fe}^{2+}/\text{Fe}^{3+}$ is commonly seen as responsible for a low resistivity in the material.

In general, the data show also that, ϵ' increases with increasing temperature and decreases with

increasing frequency as shown in Fig.(9a,b) as representative example. As temperature increases, more of the localized dipoles become free and aligned in the field direction, resulting in a small increase in ϵ' values. Since the conductivity and dielectric properties are of the same origin, therefore conductivity of samples increases with increasing temperature. This increment in conductivity is due to thermally activated drift mobility of electric charge carriers according to hopping conduction mechanism and not to the increase in number of charge carriers. Hopping of charge carriers takes place between iron ions of different valences or between iron and cobalt of different valences.



From a closer look at the data, it is observed that ϵ' diminution continuously with increasing frequency. All samples revealed dispersion due to Maxwell- Wagner interfacial polarization [34-37]. The numbers of Fe^{2+} ions on B sites, which participate in electron exchange interaction, are responsible for the polarization and maximum in case of cobalt ferrite. As the zinc, content in the mixed Co-Zn ferrites is continuously increased the number of ferrous ions on the B sites which are available for polarization decreases, resulting in a continuous decrement in the dielectric constant. This decrement in the electrical conductivity is due to the decrease in the number of Fe^{2+} ions on B sites which play a dominant role in the mechanisms of conduction and dielectric polarization [38].

The effect of n on the imaginary part " ϵ'' " of dielectric constant at different temperatures is illustrated in Fig. (10a) as a representative example. The same trend as that of " ϵ' " was obtained in " ϵ'' " relations. Such that " ϵ'' " decreases with increasing n and increases with increasing temperature in the low n region and becomes nearly independent of n at high n region. This confirms the normal dielectric behavior of all investigated samples. The variation of the loss tangent " $\tan\delta$ " with frequency at a selected temperature is illustrated in Fig. (10b) as a representative example. It is obvious that " $\tan\delta$ " is found to decrease with increasing frequency. In the low " n " region and low temperature, " $\tan\delta$ " has small values and increases rapidly with increasing temperature, while in the high " n " region " $\tan\delta$ " becomes frequency independent. This behavior may be accepted the fact, that the dielectric loss in all the investigated samples is only due to the conduction process.

Electrical conductivity

Figure (11a) represents ac conductivity (σ_{AC}) and reciprocal of absolute temperature for samples $\text{Co}_{0.6}\text{Zn}_{0.4}\text{Fe}_{1.5}\text{Cr}_{0.5}\text{O}_4$. From this figure, it is noticed that the investigated sample show a semiconductive behavior, where " σ_{AC} " increases with increasing temperature. These results agree well with many authors [36, 39,40]. Moreover, more than one straight line with different slopes was observed indicating the presence of different conduction mechanisms. The increase in conductivity was ascribed to thermally activated mobility. The slope of the low temperature region was less than that of the high temperature region, which was expected as the result of increasing thermal agitation in the high temperature region with the result of increasing electron phonon scattering. On other hand, the conductivity is likely to be weakly temperature dependence in low temperature region while it exhibits strong temperature dependence in high temperature range. In this case, it worth mentioning that, the increase of $\ln \sigma_{AC}$ with temperature may be attributed to the increase in the drift velocity and hopping frequency of the charge carriers with increasing temperature according to the relation

$$=ne \quad (12)$$

where " e " is the electronic charge and μ is the mobility of the charge carrier and " n " is the total number of charge carriers per unit volume. Also, the number of charge carriers is given by

$$n=n_e+n_h \quad (13)$$

where " e " and " h " refer to the n- and p-type charge carrier respectively.

On the other hand, variation of the electrical conductivity with frequency and temperatures is shown in Fig. (11a,b), in which conductivity is increasing calmly at low frequency and becomes frequency independent at high frequency. This behavior can be explained based on the cation distribution among A- and B- sites. In the present work, the system $\text{CoFe}_{1.5}\text{Cr}_{0.5}\text{O}_4$, possesses a partially inverse spinel as indicated from X-ray work where both of " Fe and Co " ions occupy A and B sites. In this case, the presence of $\text{Co}^{3+}/\text{Co}^{2+}$ ions given rise to p-type carriers. Then the net polarization arises from the local displacement of p-type carriers in addition to n-type carriers (exchange between $\text{Fe}^{3+}/\text{Fe}^{2+}$) since the mobility of n-type carriers is larger than that of p-type carriers [41]. So, electron hopping between Fe^{2+} and Fe^{3+} and hole hopping between Co^{3+}

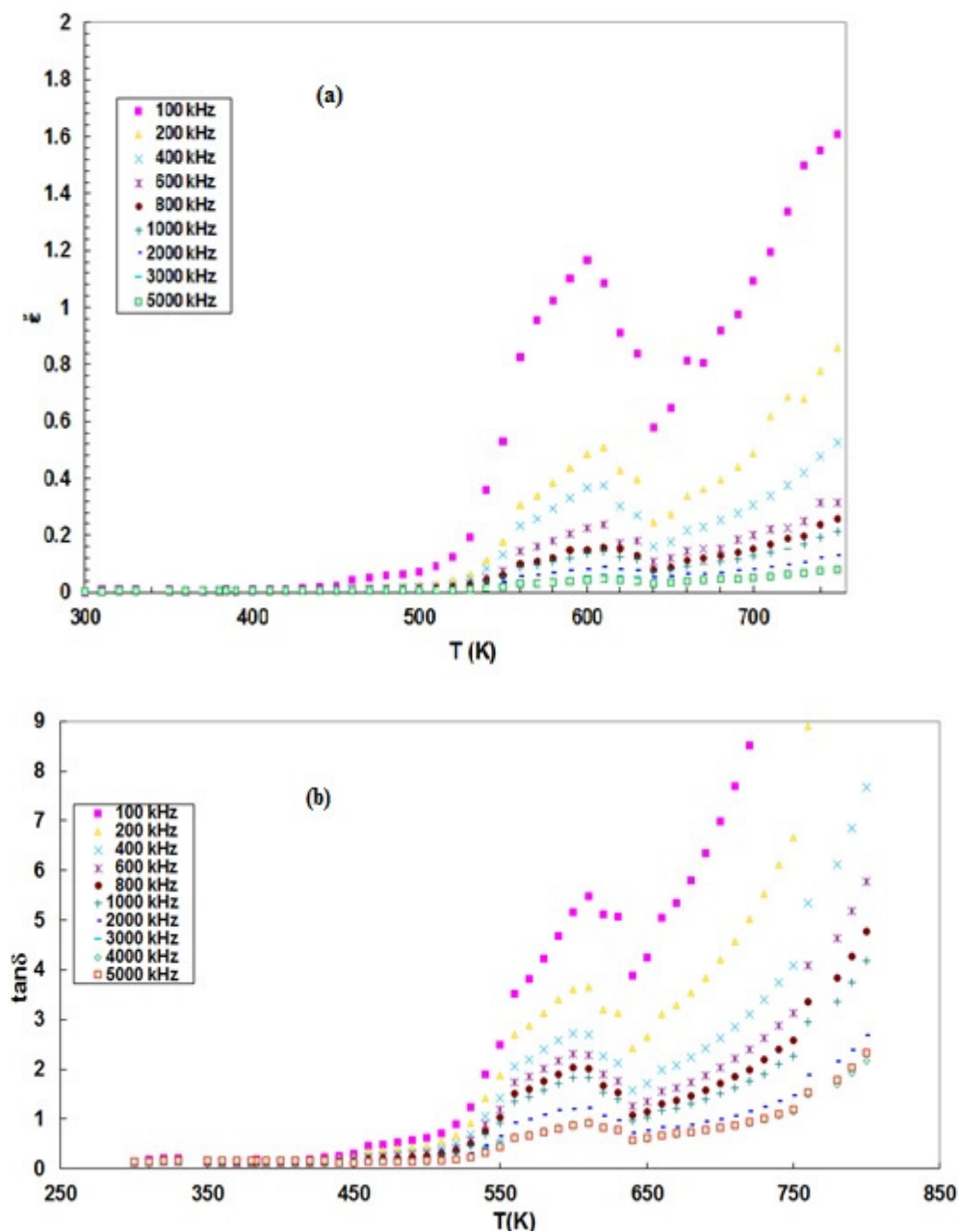
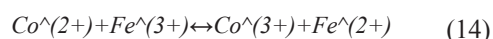


Fig.(10b): Relation between dielectric loss angle $\tan \delta$ on the absolute temperature as a function of the applied frequency for the sample $\text{Co}_{1-x}\text{Zn}_x\text{Fe}_{1.5}\text{Cr}_{0.5}\text{O}_4$, with $x=0.6$.

and Co^{2+} are responsible for electric conduction and dielectric polarization in the investigated system with $x = 0.0$. Therefore, the chance of the following reaction may exist:



The above assumption is valid only for $x = 0.0$, where the “Co” ions occupy the B site, but when “x” takes other values more than zero by substituting the magnetic “Co” ions by non-

magnetic “Zn” ions, which strongly prefers the tetrahedral site. This will force the “Fe” ions to migrate from A- sites to B- sites and the “Co” ion from B- sites to A- sites and the structure becomes normal spinel. This may lead to considering the mechanism of conduction and dielectric polarization in the investigated system to be an electron hopping between Fe^{2+} and Fe^{3+} (n-type semiconductor ferrite).

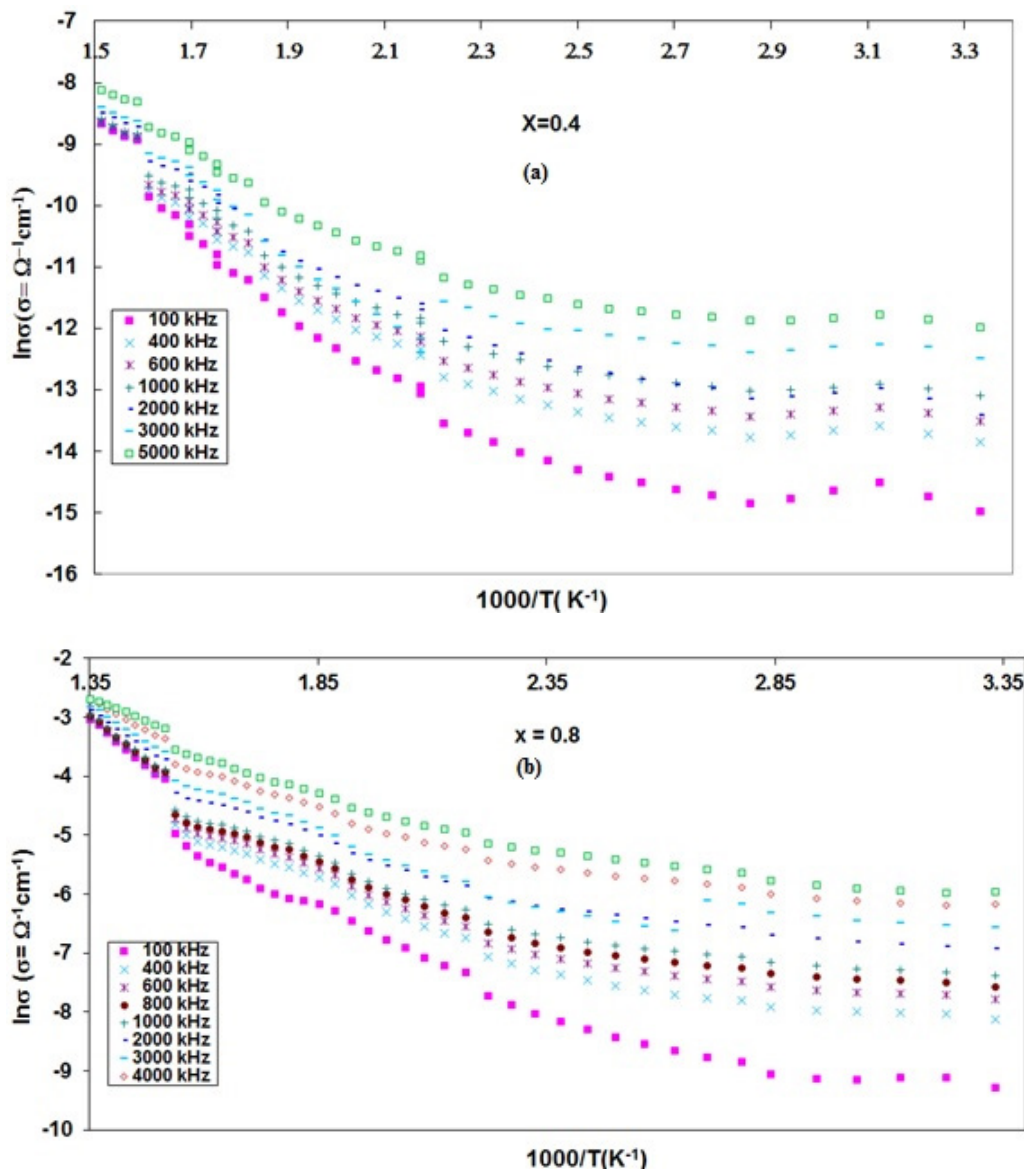


Fig. (11a,b) : Relation between electrical conductivity and reciprocal of absolute temperature for the samples $\text{Co}_{1-x}\text{Zn}_x\text{Fe}_{1.5}\text{Cr}_{0.5}\text{O}_4$, with $x = 0.4, 0.8$, at different frequencies

Magnetic Properties

Figure (12) represents a room temperature hysteresis loop for the prepared compounds, all specimen display a normal S-shape type, the size and the shape of the hysteresis curves for a magnetic material are of considerable practical importance [42]. The hysteresis loops closed at low fields and saturation magnetization (M_s) has been reached at 20000 Gauss. The saturation magnetization (M_s), remnant magnetization (M_r) and coercivity (H_c) are summarized in Table (4), H_c and M_r values are strongly dependent on x . The saturation magnetization increases slightly

with increasing Zn^{2+} up to $x=0.4$, then decreases slightly for $x=0.6$ followed by an acute decrease as x is increased, being 7.25 emu/g, 1.82 emu/g, for $x=0.8, 0$ and 1.0 respectively, (Table 4). These results agreed with the results of A. Franco, and F. C. e Silva [43] who found that an increase in the saturation magnetization of $\text{Co}_{1-x}\text{Zn}_x\text{Fe}_2\text{O}_4$ up to $\text{Zn}=0.2$ followed by a decrease as Zn increase. The increment in M_s can be explained by Neel's theory [44] of two sub-lattice model of ferrimagnetism in which A-B superexchange interaction is prevailing than the other two types of interactions (A-A& B-B)[45]. Based on the cation

distribution results tabulated in (Table 1) and due to the marked superexchange interaction between A- and B-sites (up to $x=0.2$) the magnetization is heightened. In the chemically jumbled system, spin canting is locally dependent upon analytical distributions of magnetic adjoining ions rather than to be uniform. Therewith the magnetization decrement for $x \geq 0.4$ is mainly correlated with canting of the magnetic moments. The values of the squareness (remanence ratio) which are (M_r/M_s) tabulated in Table (4) ranges from 0.0033 to 0.2947 is less than 0.5 indicated that the uniaxial surface anisotropy contribution produced by the internal strain [46, 47] or there is a formation of multidomain structure in the material.

Conclusion

A series of single-phase zinc doped cobalt chromium ferrite was synthesized by co-precipitation method. Rietveld refinement for the observed powder pattern reveals that with increasing zinc content the unit cell dimension increases, while the crystallite size increases and then decreases. The anomaly at the behavior of crystallite size was interpreted using the surface energy concept. The tetra-tetra lattice distance was found to increase with increasing Zn. The optical properties proved two energy gaps (E_{g1} and E_{g2}) for this ferrite, both E_{g1} and E_{g2} increase with increasing Zn content till $x=0.8$ and then decrease at $x=1$. may be attributed to an energy

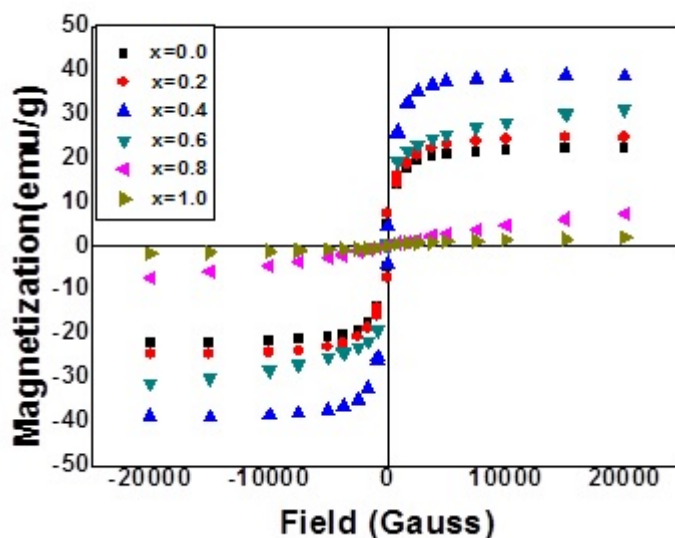


Fig. 12. Relation between magnetization and field for $\text{Co}_{1-x}\text{Zn}_x\text{Fe}_{1.5}\text{Cr}_{0.5}\text{O}_4$ ($0 \leq x \leq 1$).

TABLE 4. The saturation magnetization (M_s), Coercivity (H_c), Squareness (M_r/M_s) and remnant magnetization (M_r), are obtained at RT.

X	M_s emu/g	Coercivity (H_c) G	Squareness M_r/M_s	remnant magnetization (M_r) emu/g
0.0	22.051	212.03	0.2143	4.7257
0.2	24.686	284.07	0.2947	7.2738
0.4	38.969	121.29	0.1108	4.3179
0.6	31.210	16.599	0.0126	0.39247
0.8	7.2548	34.499	0.0033	23.758E-3
1	1.8160	208.11	0.0693	0.12590

band gap is influenced by different factors, such as crystallite size, structural parameter, and impurities. The measured transport properties revealed that the real part of dielectric constant decreases with increasing frequency and increases with increasing temperature. AC conductivity " σ_{AC} " of samples increases with increasing temperature showing a semiconducting behavior. From the magnetic measurements we found that the saturation magnetization (M_s) increases as Zn content increases up to $Zn=0.4$, then decreases with increasing Zn. This increment in M_s was explained by Neel's theory of two sub-lattice model of ferrimagnetism, while the decreasing in M_s associated with canting of magnetic moment.

References

- Bhukal S., Namgyal T., Mor S., Bansal S., Singhal S., *J. Molec. Struct.*, 1012, 162–167 (2012).
- Rajaram R. R., Serman A., *J. Chem. Soc. Faraday Trans.*, 181, 2577 (1985).
- Horvath M. P., Microwave application of soft ferrite. *J. Magn. Magn. Mater.* 215–216, 171 (2000).
- Gabal M. A., Al Angari Y. M., *Mater. Chem. Phys.*, 115, 578 (2009).
- Saafan S. A., Assar S. T., Moharram B. M., El Nimr M. K., *J. Magn. Magn. Mater.*, 322, 628 (2010).
- SLICK P. J., "Ferromagnetic Materials", 2, edited by E. P. Wohlfarth, Amsterdam (1980).
- Abraham T., *Amer. Ceram. Soc. Bull.*, 73, 862-865 (1994).
- Auzans E., Zins D., Blums E. and Massart R. *J. Mater. Sci.*, 34, 1253-1260 (1999).
- Salah L. M., Moustafa A. M. and Ahmed Farag I. S., *Ceram. Intern.*, 38, 5605–5611 (2012)
- Naverotsky A. and Kelppa O. J., *J. Inorg. Nucl. Chem.*, 29, 2701-2714 (1967).
- Rodriguez-Carvajal J., "Short Reference Guide of the Full Prof Prog., version 3.5", Laboratory Leon Brillouin (CEA-CNRS), (2006).
- Hansson A. N., Linderoth S., Mogensen M. and Somers M. A. J., *J. Alloys and Comp.*, 402, 194-200 (2005).
- Sileo E. E., Rodenas L. G., Santos C. O. P., Stephens P. W., Morando and P. J., Blesa M. A., *J. Sol. Stat. Chem.*, 179 (7), 2237-2244, (2006).
- Hakim M. A., Nath S. K., Sikder S. S., Maria K. H., *Journal of Phys. and Chem. of Soli.*, 74(9), 1316-1321 (2013).
- Vasambekar P. N., Kolekar C. B. and Vaingankar A. S., *Mater Chem. and Phys.*, 60 (3), 282-285 (1999).
- Raut A. V., Barkule R. S., Shengule D. R., Jadhav K. M., *J. Magnet. and Magn. Mater*, 358-359: 87–92 (2014).
- Moustafa A. M., Ahmed Farag I. S., Abdellatif M. H. and Ahmed M. A., *J. Mater. Sci. Mater in Electr.*, 30 (22), 20099–20108 (2019).
- Kim C. S., S. Lee W., Park S. I. and Oh J. Y., *J. Appl. Phys.*, 79, 5428–5430 (1996).
- Mc Clure D. S., "J. Phys. Chem. Solids", 3, 311-317 (1957).
- Fievet F., Germe P., De Bergvin F. and Figlarz M., *J. Appl. Cryst.*, 12, 387-394 (1979).
- Vergang F., *Phil J., Mag.*, 31, 537-550 (1975).
- Wasserman H. J. and Vermaak J. S., *Surf. Sci.*, 22, 164 – 172 (1970).
- Eckertova L., "Physics of Thin Films", Plenum press, New York, p. 306 (1986).
- Chikazumi S. and Graham C. D., "Physics of ferromagnetism" oxford university press, Oxford Oxford ; New York : Oxford University Press, (2009).
- Gad S. A., El Komy G. M., Moustafa A. M. and Ward A. A., *Indian J. Phys* 93(8), 1009–1018 (2019).
- Gad S. A. and Moustafa A. M., *Indian J. Phys.*, 90(8), 903–908 (2016).
- Gad S. A., Moustafa A. M., Ward A. A., *J. Inorg. Organomet. Polym.*, 25, 1077–1087 (2015).
- Gad S. A., Moustafa A. M., *J. Inorg. Organomet. Polym.*, 26, 147–153 (2016).
- Chand P., Gaur A., Kumar A., *Int. J. Chem. Mol. Nucl. Mater. Metall. Eng.*, 8, (12), 1203–1206 (2014).
- Caglar M., Ilican S., Caglar Y., Yalkuphanogh F., *J. Mater. Sci: Mater. Electr.*, 19, 704–708 (2008).
- Hannachi L., Bouarissa N., *Physica B*, 404, 3650–3654 (2009).

32. Ravindra N.M., Srivastava V.K., **Infrared Phys. Infrared Phys.**, 19, 603–604 (1979).
33. Anani M., Mathieu C., Lebid S., Amar Y., Chama Z., Abid H., *Comput. Mater. Sci.*, 41, 570–575 (2008).
34. Pillai V. and Shah D. O., *J. Magn. Magn. Mater.*, 163, 243-248 (1996).
35. Maxwell J. C., "*Electricity and Magnetism*", 1, Oxford University Press, New York (1973).
36. Hossain, M. S., et al., *J. Adv. Dielect.*, 8, 4, 1850030, (2018) .
37. Reddy A.V. R., Mohan G. R. and Ravinder D., *J. Mater. Sci.*, 34(13), 3169-3176 (1999).
38. Hippel A. V., "*Dielectric Materials and Applications*", Aretch House, Boston-London (1995).
39. Zaki H. M., *Physica B*, 363, 232-244 (2005).
40. Bottger H. and Bryksin V. V., "Hopping Conduction in Solids", Berlin (1985).
41. Bellad S. S. and Chougule B. K., *Mater. Chem. Phys.*, 66, 58 -63 (2000).
42. Deraz N. M. , *J. of Alloy. Compod.*, 501, 317-325 (2010)
43. Franco Jr A., and Silva F. C. E., *J. App. Phys.*, 113, 17 B, 513 (2013).
44. Neel L., *Ann. Phys.*, 12(3), 137-198 (1948).
45. R. A. Pawar,^a Sunil M. Patange,^b A. R. Shitre,^c S. K. Gore,^d S. S. Jadhav and Sagar E. Shirsath, *RSC Adv.*, 2018, 8, 25258.
46. Davis K. J. , Wells S. , Upadhyay R. V. , Charle S. W. , O'Grady K. O. , El Hilo M., Meaz T. and Morup S. , *J. Magn. Magn. Mater.*, 149, 14 -18 (1995) .
47. Ammar S., Helfen A., Jouini N. , Fiévet F. , Rosenman I. , Villain F.E. , Molinié P. and Danot M. , *J. Materi. Chem.*, 11, 186-192 (2001).

تم تحضير سلسلة من فريتات الحديد والكوبالت المغزليه المطعمه بالزنك ودراسة خصائصها التركيبية والضوئية وخصائصها الانتقالية بواسطة حيود الأشعه السينيه، الأنعكاسية الناشرة ، الخواص الكهربيه المتردده ومنحنى التخلف المغناطيسي. تحليل نتائج حيود الأشعه السينيه أثبت أن كل العينات المحضره تتكون من طور واحد هو فريتات الكوبالت المغزليه. تنقية حيود الأشعه السينيه بواسطة طريقة ريتفيلد أشارت الي زيادة أبعاد الوحده البنائيه نتيجة للأشابه (إحلال جزء من كاتيون الزنك مكان الكوبالت) وهجرة كاتيون الحديد الثلاثي من الموقع أ الي الموقع ب. تم حساب فجوات الطاقة الضوئية ووجد أن كلا من Eg1 و Eg2 يزداد مع زيادة محتوى الزنك. كما أثبتت قياسات الموصلية الكهربيه المتردده زيادة ثابت العزل الحقيقي والتخيلي بزيادة درجات الحرارة وانخفاضهما بزيادة قيمة التردد المطبق، ويمكن تفسير هذا الشذوذ من خلال نموذج مكون من طبقتين من ماكسويل فاجنر. كشفت القياسات المغناطيسية أن مغنطة التشبع تزداد مع زيادة محتوى Zn حتى قيمة إحلال 0.4 زنك ثم بعد ذلك تقل قيمة التشبع المغناطيسي.